American Mineralogist, Volume 110, pages 1626–1639, 2025

Rare occurrence of jarosite-alunite solid solutions with intermediate Al-Fe contents in the Jurassic Aztec Sandstone, Nevada, U.S.A.

Thomas M. McCollom[1,*], Sally L. Potter-McIntyre[2], Chris Donaldson[1], Andres Reyes[1], Bruce Moskowitz[3], and Peter Solheid[3]

[1]Laboratory for Atmospheric and Space Physics, University of Colorado, Boulder, Colorado 80309, U.S.A.
[2]School of Earth Systems and Sustainability, Southern Illinois University, Carbondale, Illinois 62901, U.S.A.
[3]Department of Earth and Environmental Sciences and Institute for Rock Magnetism, University of Minnesota, Minneapolis, Minnesota 55455, U.S.A.

Abstract

Experimental studies have demonstrated that solid solutions of minerals from the alunite group, with chemical compositions intermediate between the Al and Fe end-members, can be readily synthesized in the laboratory. In contrast, up until about a dozen years ago, there were no confirmed reports of alunite group minerals with intermediate Al-Fe compositions in natural settings, leading some to suggest that minerals with such compositions might not exist in nature. In recent years, however, alunite group minerals with intermediate Al-Fe compositions have been documented in a few isolated locations, which were previously limited to basalt-hosted acid-sulfate fumarole deposits and acid mine drainage pit lakes. These occurrences contrast with nearly all other reports of minerals from this group, whose measured chemical compositions are very close to either the Al or Fe end-members. Here, we report jarosite-alunite solid solutions containing approximately equal amounts of Al and Fe, which are found in mineralized fractures of the Aztec Sandstone in southeast Nevada. Analysis of the minerals by X-ray diffraction, Raman spectroscopy, and visible-near infrared spectroscopy confirms that they are bona fide solid solutions and not intimate mixtures of end-member minerals. This study represents the first documented occurrence of alunite group solid solutions with intermediate Al-Fe compositions in sedimentary rocks. The results further demonstrate that alunite group minerals with a wide range of Al-Fe compositions occur naturally and can persist for millions of years or more in natural systems.

Keywords: Jarosite, alunite, solid solution, sulfate minerals, sedimentary rocks, Aztec sandstone

Introduction

Minerals in the alunite group have an ideal chemical formula of $AB_3(SO_4)_2(OH)_6$, where the *A* site is most commonly occupied by the monovalent ions K^+, Na^+, and H_3O^+ (hydronium) and the *B* site is occupied predominantly by Al^{3+} and Fe^{3+} (Jambor 1999; Stoffregen et al. 2000; Dutrizac and Jambor 2000; Papike et al. 2006b; Mills et al. 2009). Members of this group with Al > Fe can be classified in the alunite subgroup, while those with Fe > Al comprise the jarosite subgroup (Fig. 1a). Structurally related minerals in the broader alunite supergroup encompass the substitution of PO_4 or AsO_4 for SO_4, which is typically accompanied by increased incorporation of divalent cations such as Ca and Pb in the *A* site (Jambor 1999; Papike et al. 2006b; Mills et al. 2009).

Within the alunite group itself, the potential for the *A* and *B* sites to be occupied by several different cations raises the possibility of crystallization as solid solutions containing mixtures at these sites. Solid solution mixing of K^+, Na^+, and H_3O^+ (as well as other cations) in the *A* site is widespread in natural samples, and has also been extensively studied using synthetic solid solutions (e.g., Brophy and Sheridan 1965; Ripmeester et al. 1986; Stoffregen and Cygan 1990; Stoffregen and Alpers 1992; Polyak and Güven 1996; Stoffregen et al. 2000; Dutrizac and Jambor 2000; Deyell and Dipple 2005; Juliani et al. 2005; Papike et al. 2006a, 2006b, 2007; Basciano and Peterson 2007, 2008; Burger et al. 2009; Holley et al. 2016; Whitworth et al. 2020). The wide range of solid solution mixing in the *A* site is illustrated in Figure 1a, which shows a summary of measured alunite group mineral compositions compiled from the literature (black diamonds). The measured compositions exhibit a wide range of K/(K + Na) ratios, reflecting a complete range of mixing of K and Na on the *A* site. Note also that many of the measured compositions included in the compilation have (K + Na) < 1 atoms per formula unit (pfu), indicating the *A* sites also include H_3O^+ (Stoffregen et al. 2000), which adds to the broad extent of solid solution mixing on this site.

In contrast to the extensive solid solution mixing observed in the *A* site, reports of solid solutions of alunite group minerals from natural samples that contain mixtures of Al and Fe in the *B* site have been extremely limited (e.g., Scott 1987; Stoffregen et al. 2000). As shown by the black diamonds in Figure 1a, nearly all measured compositions of alunite group minerals have Al and Fe contents that are close to the end-members (i.e., alunite subgroup minerals with <10 mol% Fe-for-Al substitution or jarosite subgroup minerals with <15 mol% Al-for-Fe substitution). As first noted by Brophy et al. (1962), alunite subgroup minerals typically contain very little Fe, even when they precipitate in iron-rich environments. Even in environments where minerals from

* Corresponding author E-mail: mccollom@lasp.colorado.edu Orcid https://orcid.org/0000-0002-3596-5588

0003-004X/25/0010–1626$05.00/DOI: https://doi.org/10.2138/am-2024-9423

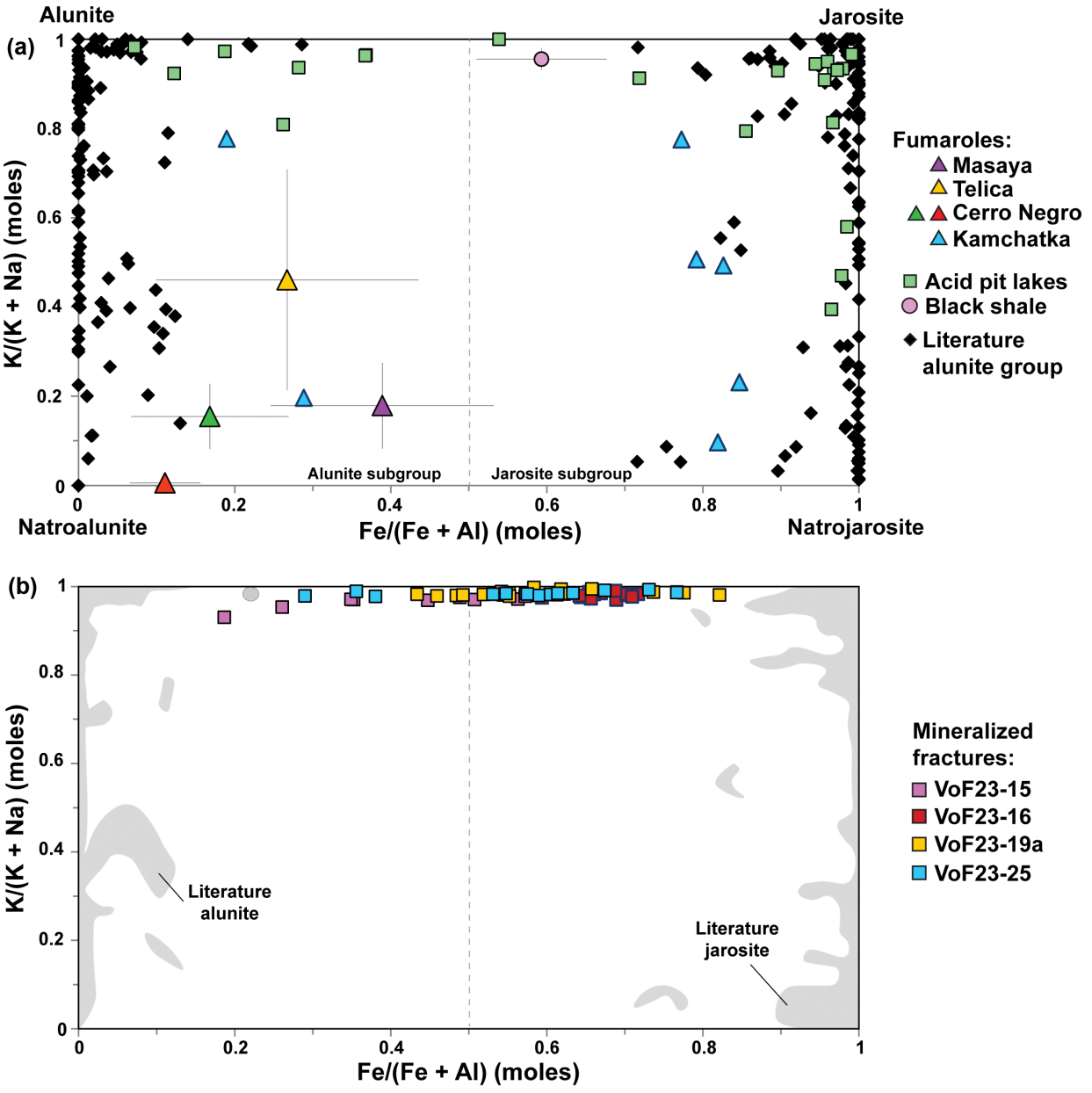

Figure 1. Quadrilateral diagram for alunite group minerals showing the relative proportions of K and Na molecules in the *A* site and proportions of Al and Fe molecules in the *B* site (after Papike et al. 2006a, 2006b). Corners of the quadrilateral represent ideal end-member compositions for stoichiometric alunite and jarosite subgroup minerals, as labeled. (**a**) Data for natural samples from previous studies. (**b**) Measured compositions of jarosite-alunite solid solutions from mineralized fractures in the Aztec Sandstone (this study). The black diamonds in (**a**) represent a compilation of published chemical compositions for alunite group minerals from 32 separate studies and include >245 measurements from 62 sample localities (McCollom 2024). The data set encompasses a broad spectrum of geologic environments that includes: supergene and hypogene hydrothermal deposits, fumaroles, acid mine drainage sites, acid-saline lakes, shales, a martian meteorite, intertidal algal mats, soils, and laterites. (Note: In this context, the large majority of studies that report the presence of alunite group minerals in geologic samples provide incomplete or no information on their chemical composition, so their compositions in many settings are unknown.) Triangles in (**a**) represent average values for JASS in active acid-sulfate fumarole deposits from Nicaragua (Masaya, Telica, Cerro Negro; McCollom et al. 2014) and Kamchatka (Zhitova et al. 2022), squares are measurements from minerals in acid pit lakes (Sánchez-España et al. 2016), and the circle represents average values for Cambrian black shale from Zuo et al. (2021; their "Type II jarosite"). For average values, vertical and horizontal black lines reflect one standard deviation from the average. In (**b**), gray areas encompass most compositions reported in the literature for alunite and jarosite subgroup minerals, excluding a couple of outliers. Note that the diagram does not account for any H_3O^+ molecules that may be present in the *A* and *B* sites. (Color online.)

the alunite and jarosite subgroups are found adjacent to one another in the same sample, they typically occur as separate mineral phases with near-end-member Al- and Fe-rich compositions rather than as solid solutions with intermediate Al-Fe compositions (e.g., Keith et al. 1979; Long et al. 1992; Alpers et al. 1992; Vasconcelos et al. 1994; Bouzari and Clark 2002; Zimbelman et al. 2005; Papike et al. 2006a, 2006b; Holley et al. 2016; Potter-McIntyre and McCollom 2018). While extensive solid solution mixing of Fe and Al in the *B* site has been observed for structurally related minerals in the broader alunite supergroup, this mixing is only found to be continuous when there was substantial (>55%) substitution of PO_4^{3-} for SO_4^{2-} as well as >80% substitution of a divalent cation into the *A* site (Scott 1987), which places these solid solutions outside of the alunite group itself.

The scarcity of alunite group minerals with intermediate Al-Fe compositions has led some authors to propose that formation of such solid solutions might be precluded in natural settings (e.g., Scott 1987; Stoffregen et al. 2000). The relatively facile synthesis of alunite group minerals with a full range of chemical compositions between the Al and Fe end-members in the laboratory (e.g., Brophy et al. 1962; Härtig et al. 1984; Drouet et al. 2004; McCollom et al. 2014) suggests that there is no inherent immiscibility gap or thermodynamic prohibition that would preclude precipitation of solid solutions with intermediate compositions. Previous studies have therefore focused on fluid chemistry to explain the dearth of Al-Fe solid solutions in natural settings rather than invoking thermodynamic or crystal structure inhibitions. For example, Stoffregen et al. (2000) attribute the scarcity of minerals with intermediate compositions to differences in the hydrolysis constants of dissolved Al and Fe species, which could potentially lead to preferential precipitation of one end-member or the other in lieu of solid solutions, depending on local environmental conditions. Others have pointed to environmental factors, such as oxidation state or pH, that might lead to the preferential precipitation of either the alunite or jarosite subgroup minerals with little or no Al-Fe substitution (e.g., Keith et al. 1979; Papike et al. 2006a, 2006b).

In recent years, however, a few cases have emerged where solid solutions of alunite group minerals with intermediate Al-Fe compositions have been reported in natural samples, with compositions occupying the middle portion of the diagram in Figure 1a. McCollom et al. (2013a, 2014) described the occurrence of Fe-rich natroalunite containing up to 40 mol% Fe in the *B* site in deposits formed by acid-sulfate alteration of basalts at active fumaroles in Central America (Fig. 1a), and solid solutions with similar intermediate Al-Fe compositions were also produced during laboratory simulations of acid-sulfate alteration of basalt (McCollom et al. 2013b). Zhitova et al. (2022) subsequently reported alunite group minerals with intermediate Al-Fe compositions in similar fumarolic settings from Kamchatka (Fig. 1a). Minerals from the alunite group with intermediate Al-Fe compositions have also been reported in pit lakes formed from acid mine drainage (Sánchez-España et al. 2016). Although the alunite group minerals in the pit lakes exhibited a range of compositions that evidently reflect fluctuating conditions (Fig. 1a), fine-scale elemental mapping showed the co-occurrence of Al and Fe, indicative of solid solutions in many crystals.

Here, we report an additional occurrence of alunite group minerals with intermediate Al-Fe compositions from the Aztec Sandstone in southeastern Nevada, just south of Valley of Fire State Park (VoF). Since these minerals have chemical compositions intermediate between the jarosite and alunite end-members, we refer to them herein as jarosite-alunite solid solutions, or "JASS" for short. The JASS occupy pore spaces in mineralized fractures within the sandstones (Fig. 2). To our knowledge, this study is the first to describe mineralized fractures within the Aztec

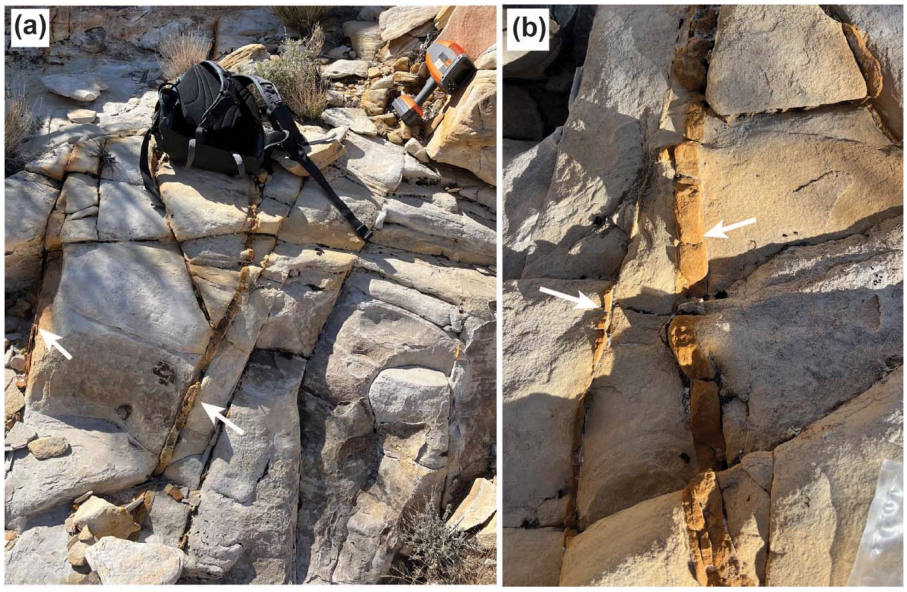

Figure 2. Examples of mineralized fractures containing jarosite-alunite solid solutions in the Aztec Sandstone (white arrows). Note the presence of many adjacent fractures and joints that are unmineralized. Backpack in (**a**) for scale. In (**b**), the mineralized fracture on the right has a diameter of about 3 cm and is the site of sample VoF23-24. Additional field images of mineralized fractures are provided in Online Materials[1] Figure S1. (Color online.)

Sandstone that are dominated by alunite group minerals, and the first to rigorously document the presence of intermediate Al-Fe solid solutions for this mineral group in sedimentary rocks.

Because alunite group minerals commonly occur as dense aggregates of very fine-grained crystals (<1 μm diameter; "porcelaneous") or display chemical and mineralogical zonation on a submicrometer scale, chemical analyses alone cannot always be relied upon to differentiate bona fide solid solutions from fine-scale intergrowths of end-member components (e.g., Desborough et al. 2010). Therefore, additional methods must be employed to verify that the minerals are solid solutions rather than intimate mixtures of end-members. In crystallography, Vegard's Law posits that substitution of an element in a crystal structure produces approximately linear variation in unit cell dimensions (Vegard 1921), and in many cases, this results in lattice parameters and spectral band positions for solid solutions that display linear trends as a function of mineral composition with values intermediate between those of the pure end-members. For example, solid solutions of sulfate minerals, including those of the alunite group, have been shown to display linear trends as a function of chemical composition for cell lattice parameters, position of X-ray diffraction peaks, and band positions in Raman and Fourier transform infrared spectra (e.g., Brophy et al. 1962; Stoffregen and Alpers 1992; McCollom et al. 2014; Cao et al. 2017; Talla and Wildner 2019; Talla et al. 2020). We show here that JASS in the mineralized fractures exhibit lattice parameters, X-ray diffraction peaks, and spectral band positions for Raman spectroscopy that are intermediate between those of Al- and Fe-end-members and consistent with their measured chemical compositions, confirming that they are bona fide solid solutions.

Geologic Setting

Rock samples were collected from the Aztec Sandstone in the Buffington Pockets area just south of Valley of Fire State Park near Overton, Nevada (36°23′09″ N, 114°41′21″ W). The characteristics and geologic history of the Aztec Sandstone in the region have been described by Taylor et al. (1999), Flodin and Aydin (2004a, 2004b), and Eichhubl et al. (2004) and are summarized briefly here. The Aztec Sandstone is an eolian, quartz-rich subarkosic sandstone, containing about 8% K-feldspar that is variably replaced by kaolinite. The Aztec Sandstone is heavily faulted and jointed in VoF and the surrounding region, which has been attributed to Basin and Range tectonics during the Miocene (Taylor et al. 1999; Taylor and Pollard 2000; Flodin and Aydin 2004a, 2004b; Eichhubl et al. 2004). Some of the fractures are mineralized, but in previously reported cases, the fracture mineralization was found to be dominated by phyllosilicates, iron oxides, and/or carbonate minerals (Taylor et al. 1999; Eichhubl et al. 2004), rather than the alunite group minerals reported here.

Eichhubl et al. (2004) initially reported the occurrence of minor amounts of alunite and jarosite in the Aztec Sandstone at VoF and adjacent areas (including at the study site). However, Eichhubl et al. (2004) only noted the presence of these minerals in some of their samples and provided no chemical analyses or further description of the minerals. Moreover, the jarosite and alunite described by Eichhubl et al. (2004) were dispersed in the host rocks, and they do not describe any occurrences of these minerals in fractures like the ones described here. Eichhubl et al. (2004) proposed that the alunite and jarosite were deposited when deeply sourced sulfide-rich basinal fluids mixed with oxidizing meteoritic fluids, resulting in the oxidation of sulfide to sulfate and precipitation of sulfate minerals together with goethite and/or hematite. Those authors propose that the spatial distribution patterns of these minerals within the host rock in VoF were strongly influenced by enhanced fluid flow along previously formed joints and fractures.

Methods

Samples of the mineralized fractures were examined using various methods. Initial characterization of the mineralogy of the fractures was conducted using powder X-ray diffraction (XRD) with a Terra instrument (Olympus, Inc.) and Cu*K*α radiation. To focus on the composition of pore-filling minerals in the quartz-dominated sandstones, the XRD analyses were performed on a fine-grained fraction prepared by lightly grinding the bulk samples in a ceramic mortar and pestle, followed by sieving to obtain the <53 μm fraction. Calculation of unit-cell parameters based on the XRD data was performed using XPowder (https://www.xpowder.com/)

Visible-near infrared (VNIR) spectroscopy of whole rock hand samples was performed in the laboratory using a TerraSpec Halo handheld spectrometer (Malvern Panalytical, Inc.). The spectra were obtained from freshly exposed faces on whole-rock hand samples. Spectra were obtained over a wavelength range of 0.35–2.5 μm, with data accumulated over 50 scans. The spectral resolution is 3 nm at 0.700 μm, 9.8 nm at 1400 nm, and 8.1 nm at 2.100 μm, according to the instrument documentation. The spectra shown were processed using the proprietary software provided with the instrument, with no background subtraction.

Morphological and textural characterization of the samples, as well as initial chemical analyses of mineral phases, were performed by scanning electron microscopy coupled with energy-dispersive X-ray spectroscopy (SEM/EDS). The analyses were performed with a Hitachi SU3500 SEM equipped with an Oxford Instruments EDS and AZTEC data processing software. Observations were made on both polished thin sections and on small rock pieces mounted on Al stubs using carbon tape. More detailed chemical compositions of the JASS and associated minerals were obtained using electron microprobe analysis (EMPA) of polished thin sections. The measurements were performed using a JEOL 8230 electron microprobe with a beam energy of 15 keV, a beam current of 10 nA, and a beam diameter of 1 μm. By convention, measured chemical compositions of alunite group minerals are converted to molecular formulas by assuming two $\Sigma(SO_4 + PO_4)$ per formula unit (pfu) and adjusting the abundances of other elements proportionally (e.g., Stoffregen et al. 2000), and that convention is followed here (see Online Materials[1] Data set 1 for calculations).

Chemical compositions of bulk rock powders were analyzed at Activation Laboratories Ltd. (Ancaster, Canada) using a combination of inductively coupled plasma optical emission spectroscopy (ICP-OES) and instrumental neutron activation analysis (INAA). Sulfate was analyzed separately using infrared detection during the combustion process. Isotopic analysis of S and O in sulfate minerals was also performed by Activation Laboratories. In most cases, the chemical and isotope analyses were performed on the fine-grain fractions of powdered rocks to focus on the compositions of the secondary pore-filling materials, prepared as described above for XRD analysis.

Mössbauer spectroscopy (MS) was performed at room temperature in zero applied magnetic field using a conventional constant-acceleration spectrometer (model MS6, SeeCo, U.S.A.) in transmission geometry with a ^{57}Co/Rh source. Spectra were obtained using a triangular waveform and a 1024-channel analyzer. An α-Fe foil at room temperature was used to calibrate isomer shifts and velocity scale. Mössbauer spectra were fit by least-squares to sums of Lorentzian lines using custom software to obtain estimates for isomer shift (IS), quadrapole splitting (QS), hyperfine field (B_{HF}), linewidth (Γ), and relative area (A) for each subspectrum. Spectra were collected using bulk samples. Low-temperature remanent magnetization was measured with a superconducting quantum interference device magnetometer (Quantum Design, San Diego, California; MPMS-XL).

Raman spectra were collected using a Horiba LabRAM HR Evolution Raman spectrometer. Measurements were acquired using a 532 nm excitation laser at 50% or 100% power, 600 mm^{-1} diffraction grating, 50× long working distance microscope objective, and 5 s laser acquisition times with 5 spectra accumulations,

equating to 25 s of laser focus per spectra acquired. The spectrometer was calibrated using the 520 cm^{-1} Raman peak of a reference Si sample prior to analysis. Results shown here were background subtracted.

For comparison with the natural samples, several synthetic solid solutions of alunite group minerals with intermediate Al-Fe compositions were prepared using methods described in the Online Materials[1]. The products were analyzed using the same methods as the natural samples. Mineral stability diagrams were constructed with the aid of the Act2 component of Geochemist's Workbench, version 11.0.8 (Aqueous Solutions LLC). The calculations utilized the thermo.com.V8.R6+ database supplied with the software, which was modified by the addition of data for the alunite group solid solution, as described in the Online Materials.

Results

Occurrence and habit of jarosite-alunite solid solutions

The jarosite-alunite solid solutions with intermediate Al-Fe compositions were found in mineralized fractures that crosscut Aztec Sandstone (Fig. 2; Online Materials[1] Fig. S1). The mineralized fractures are typically dark tan in color and, where exposed by erosion, many of the mineralized fractures form a dark brown-to-black surface coating (e.g., Online Materials[1] Figs. S1a and S1f). The fractures have mineralized selvages that extend up to ~3 cm into the host rock and have exposed lengths ranging from <1 to >30 m. The mineralized fractures and selvages exhibit sharp boundaries with the adjacent unmineralized host rocks. In most samples, few alunite group minerals were found in the pore spaces of the host sandstone outside of the mineralized regions.

The JASS occupy pore spaces between larger quartz and K-feldspar grains (Fig. 3; Online Materials[1] Figs. S2 and S3). Identification of the minerals as members of the alunite group was confirmed by XRD and Raman spectroscopy (Online Materials[1] Figs. S4 and S5). The JASS have a pseudocubic morphology, with diameters ranging from <1 to ~15 μm, and they are the most abundant cement mineral, by far, within the pores. Other cement minerals commonly observed in the pore spaces (albeit in substantially lower abundances) included calcite, an unidentified Ca-phosphate mineral with a molar Ca:P ratio of ~1.8 (presumably apatite), and unidentified Fe-oxides/oxyhydroxides. The calcite and Ca-phosphate typically envelop the JASS, indicating that they precipitated after the JASS crystals were already present (Figs. 3e and 3f; Online Materials[1] Figs. S2a and S2c). The Fe-oxides/oxyhydroxides were consistently found to contain small amounts of Si, Al, P, S, and Mg in addition to Fe (Online Materials[1] Fig. S6). Thin gray zones found within a couple of the mineralized fractures contained spherules composed of hematite (Online Materials[1] Fig. S2f); these spherules are the subject of ongoing study and will be described in a separate communication.

Chemical compositions of JASS

Average chemical compositions of JASS from several representative mineralized fractures as determined by EMPA are summarized in Table 1, with more comprehensive analyses provided in Online Materials[1] Data set 1. Average molecular formulas for the JASS based on the EMPA measurements are provided in Table 2. The relative proportions of Al and Fe in the JASS from several individual EMPA analyses are also illustrated in Figure 1b. Chemical compositions of co-occurring calcite, Ca-phosphate, and Fe-oxides/oxyhydroxide are provided in Online Materials[1] Table S1.

As seen in Figure 1b, the JASS in the mineralized fractures contain intermediate Al-Fe compositions, corresponding to average Fe# [Fe# = 100 × Fe/(Al+Fe), mole basis] between

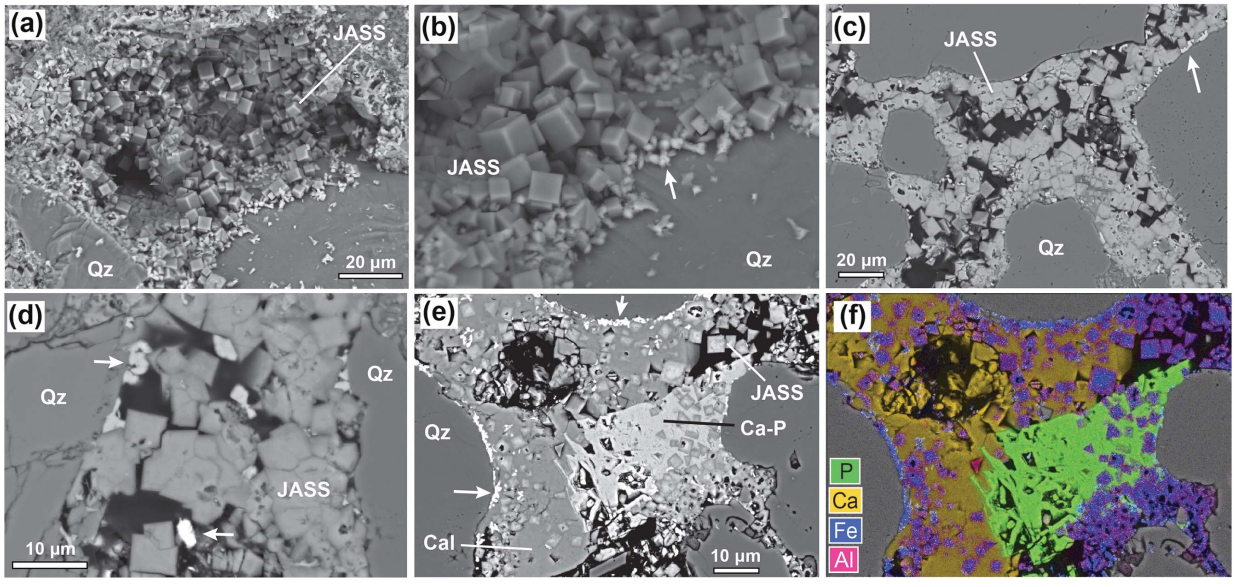

Figure 3. Backscattered electron images of pore-filling secondary minerals in mineralized fractures. (**a**) Pseudocubic jarosite-alunite solid solution crystals occupying an exposed pore space. (**b**) Enlarged view from (**a**). (**c**,**d**) Typical cross sections of pore-filling JASS from thin sections. (**e**,**f**) Calcite and Ca-phosphate minerals surrounding JASS crystals in pore space, with element map shown in (**e**). White arrows point to examples of unidentified Fe-oxide/hydroxide minerals (bright crystals in images). Additional examples and context images are provided in Online Materials[1] Figures S2 and S3. Mineral abbreviations: Qz = quartz; Cal = calcite; JASS = jarosite-alunite solid solutions; Ca-P = unidentified Ca-phosphate. Samples shown: (**a**,**b**,**e**,**f**) VoF23-19a, (**c**,**d**) VoF23-24. (Color online.)

Table 1. Representative average chemical compositions (in weight percent) for alunite group minerals in mineralized fractures and host rocks

Sample	VoF23-15 (n = 12)	VoF23-16 (n = 13)	VoF23-19a (n = 17)	VoF23-25 (n = 13)	VoF23-44 (n = 1)	VoF17-T11 (n = 17)	VoF23-11 (n = 4)
Sample type	Fracture	Fracture	Fracture	Fracture	Fracture	Host rock	Host rock
mineral	JASS	JASS	JASS	JASS	Alunite	Jarosite	Jarosite
SiO_2	1.0 (0.7)	0.8 (0.7)	0.4 (0.3)	0.3 (0.5)	1.9	0.7 (0.4)	1.4 (0.9)
Al_2O_3	16.5 (4.7)	10.0 (1.2)	12.5 (3.8)	13.7 (5.0)	34.2	1.9 (0.5)	2.8 (0.6)
Fe_2O_3	21.0 (6.0)	31.8 (1.5)	29.7 (5.4)	26.9 (6.0)	0.9	41.6 (1.1)	39.4 (1.7)
MgO	b.d.	b.d.	b.d.	b.d.	b.d.	b.d.	b.d.
CaO	1.0 (1.0)	0.3 (0.1)	b.d.	b.d.	0.6	b.d.	b.d.
Na_2O	b.d.	b.d.	b.d.	b.d.	b.d.	b.d.	b.d.
K_2O	6.6 (0.8)	5.2 (0.9)	5.0 (0.8)	6.4 (1.6)	6.8	7.5 (1.4)	6.5 (1.8)
TiO_2	b.d.	b.d.	b.d.	b.d.	-	b.d.	b.d.
P_2O_5	4.6 (2.9)	2.7 (0.4)	1.9 (0.8)	2.0 (0.5)	2.4	3.0 (0.6)	3.2 (0.4)
SO_3	26.7 (2.0)	30.7 (0.7)	31.7 (1.1)	32.3 (1.1)	34.3	28.4 (1.1)	27.5 (1.4)
Sum	77.8 (3.3)	81.7 (1.4)	83.3 (2.3)	81.7 (1.8)	81.5	83.2 (2.2)	81.1 (2.5)
Est. H_2O[a]	22.2	18.3	16.7	18.3	18.5	16.8	18.9
Atoms pfu[b]							
K	0.71	0.53	0.50	0.63	0.63	0.80	0.72
Na	<0.01	<0.01	<0.01	<0.01	<0.01	<0.01	<0.01
$(H_3O^+)_A$[c]	0.29	0.47	0.50	0.37	0.37	0.20	0.28
Fe	1.34	1.89	1.76	1.57	0.05	2.63	2.55
Al	1.60	0.93	1.16	1.24	2.90	0.19	0.28
$(H_3O^+)_B$[c]	0.06	0.18	0.08	0.19	0.05	0.18	0.17
P	0.31	0.18	0.13	0.13	0.15	0.21	0.23
S	1.69	1.82	1.87	1.87	1.85	1.79	1.77
Fe#	45	67	60	56	2	93	90

Notes: Oxide wt% data represent averages with standard deviation shown in parentheses; n = number of analyses included in average. "b.d." = Below detection limit of ~0.2 wt%.

[a] Estimated H_2O contents calculated as the amount required to bring the wt% total to 100.

[b] Number of atoms per formula unit (pfu) calculated assuming $\Sigma(S + P) = 2$ (e.g., Jambor 1999).

[c] Estimated number of H_3O^+ molecules per formula unit required to achieve charge balance in the *A* and *B* sites. Data for individual measurements, as well as additional samples and all calculations, are provided in Online Materials[1] Data set 1.

45 and 67 in different samples (Tables 1 and 2). Individual analyses within a single rock sample exhibited some chemical variation, although this variation was limited in extent (Fig. 1b; Online Materials[1] Data set 1). The *A* site of the JASS was predominantly occupied by K, with essentially no Na present. However, the minerals consistently had <1 K per formula unit, suggesting the presence of substantial amounts of H_3O^+ in the *A* site (Tables 1 and 2). The JASS also consistently have elevated P contents (Table 1), indicating substantial substitution of PO_4^{3-} for SO_4^{2-} (~6–15 mol%). However, there was no detectable increase in divalent cations (e.g., Ca, Pb) as is typically observed for other minerals within the alunite supergroup that contain PO_4 (e.g., Scott 1987; Jambor 1999; Papike et al. 2006b); therefore, charge balance for the PO_4^{3-} is likely accommodated by either additional H_3O^+ or substitution of H_2O for OH^- in the crystal structure (Tables 1 and 2).

In most samples, individual JASS crystals viewed in cross section showed no chemical zonation (Fig. 3). In one sample, however, some JASS crystals were observed to have cores that were relatively enriched in Al and P with rims enriched in Fe (i.e., VoF23-15; Online Materials[1] Fig. S7). In another sample that contained hematite spherules, the JASS crystals had rims that were slightly darker than the interiors in backscattered electron images, indicating higher Al and lower Fe contents (Online Materials[1] Fig. S2f). In a few other instances, examination of thin sections revealed areas where individual JASS crystals have hollow interiors (e.g., Online Materials[1] Fig. S2d), which could potentially represent redissolution of cores formed early on. In addition to the hollow interiors, there were a few areas in some samples where the JASS crystals appeared to be partially corroded; overall, however, the majority of JASS crystals seem to be fully intact with little evidence for dissolution after they formed, even where they were enshrouded by carbonate and phosphate minerals (Fig. 3; Online Materials[1] Fig. S2).

Confirmation of solid solutions

Several analytical methods were employed to confirm that the minerals with intermediate Al-Fe compositions were bona fide solid solutions, including XRD, Raman spectroscopy, and VNIR spectroscopy (Fig. 4). Each of these methods produced results consistent with solid solutions for the JASS in the mineralized fractures. Key results of the measurements are

Table 2. Average inferred molecular formulas for alunite group minerals at the study site based on the measured chemical compositions

Sample	Type	Mineral	Estimated molecular formula[a]
VoF23-15	Fracture	JASS	$(K_{0.71}H_3O^+_{0.39})(Fe_{0.45}Al_{0.53}H_3O^+_{0.02})_3(SO_4)_{1.69}(PO_4)_{0.31}(H_2O)_{0.31}(OH)_{5.69}$
VoF23-16	Fracture	JASS	$(K_{0.53}H_3O^+_{0.47})(Fe_{0.63}Al_{0.31}H_3O^+_{0.06})_3(SO_4)_{1.82}(PO_4)_{0.18}(H_2O)_{0.18}(OH)_{5.82}$
VoF23-19a	Fracture	JASS	$(K_{0.50}H_3O^+_{0.50})(Fe_{0.59}Al_{0.39}H_3O^+_{0.02})_3(SO_4)_{1.87}(PO_4)_{0.13}(H_2O)_{0.13}(OH)_{5.87}$
VoF23-25	Fracture	JASS	$(K_{0.63}H_3O^+_{0.37})(Fe_{0.52}Al_{0.41}H_3O^+_{0.07})_3(SO_4)_{1.87}(PO_4)_{0.13}(H_2O)_{0.13}(OH)_{5.87}$
VoF23-44	Fracture	Alunite	$(K_{0.63}H_3O^+_{0.37})(Fe_{0.02}Al_{0.96}H_3O^+_{0.02})_3(SO_4)_{1.85}(PO_4)_{0.15}(H_2O)_{0.15}(OH)_{5.85}$
VoF17-T11	Host rock	Jarosite	$(K_{0.80}H_3O^+_{0.20})(Fe_{0.88}Al_{0.06}H_3O^+_{0.06})_3(SO_4)_{1.79}(PO_4)_{0.21}(H_2O)_{0.21}(OH)_{5.79}$
VoF23-11	Host rock	Jarosite	$(K_{0.72}H_3O^+_{0.28})(Fe_{0.85}Al_{0.09}H_3O^+_{0.06})_3(SO_4)_{1.77}(PO_4)_{0.23}(H_2O)_{0.23}(OH)_{5.77}$

[a] Molecular formulas estimated by assuming: (1) the deficiencies of cations in the *A* and *B* sites relative to the ideal formula are accommodated by H_3O^+, and (2) charge balance from substitution of PO_4^{3-} for SO_4^{2-} is accommodated by conversion of OH groups to H_2O.

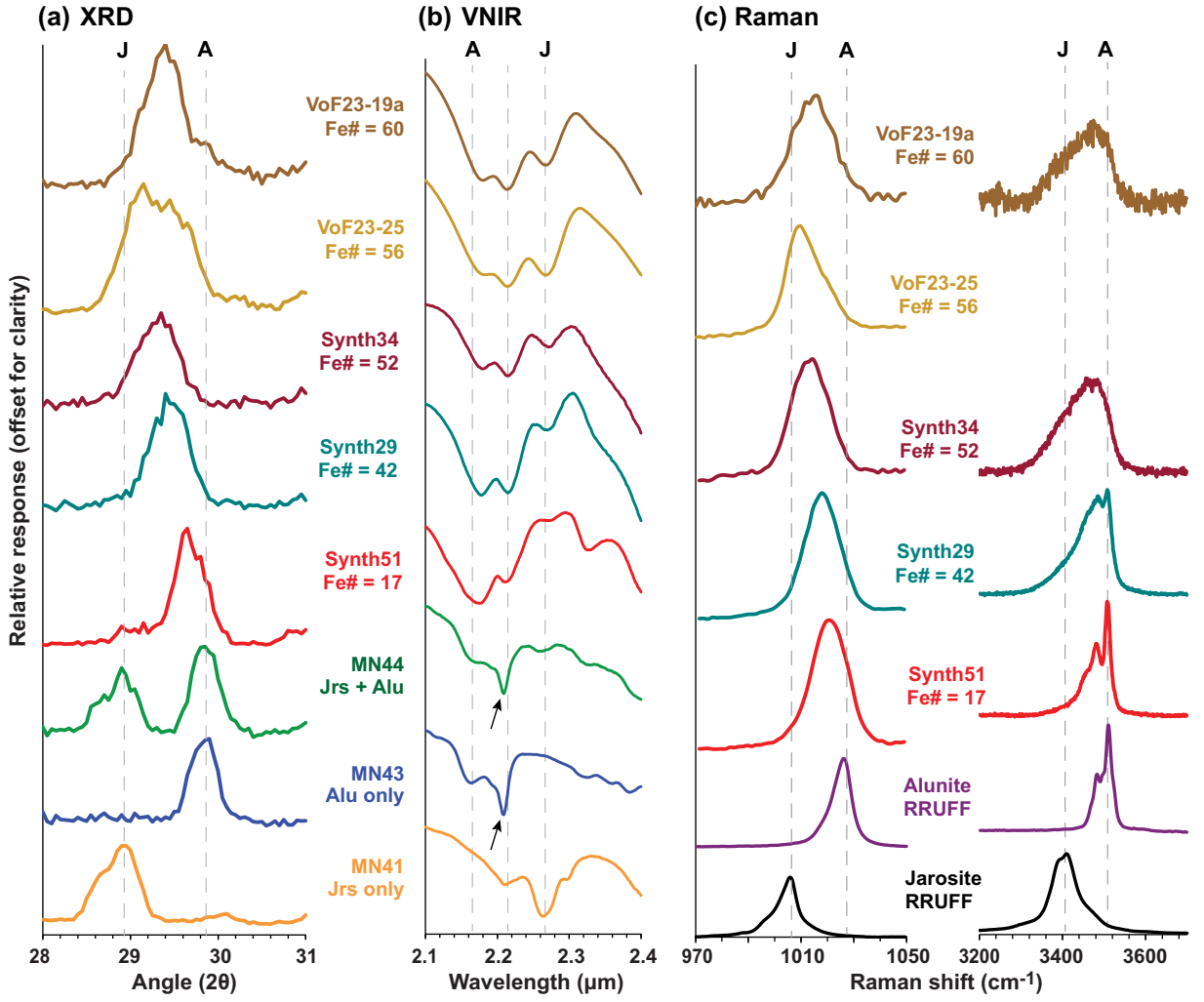

Figure 4. Highlights of analyses of jarosite-alunite solid solutions in mineralized fractures by (**a**) XRD, (**b**) VNIR spectroscopy, and (**c**) Raman spectroscopy, with results for other natural samples and synthetic solid solutions shown for reference. More complete results are provided in Online Materials[1] Figures S4, S5, and S8, and data for additional Aztec Formation samples are provided in Online Materials[1] Data set 1. Samples labeled MN41, MN43, and MN44 are jarosite- and alunite-cemented sandstones from Mollies Nipple, Utah (Online Materials[1] Fig. S9) (Potter-McIntyre and McCollom 2018). "Synth" samples are synthetic Al-Fe solid solutions produced using methods described in the Online Materials. Raman data for jarosite and alunite in (**c**) are from the RRUFF database. Abbreviations: J = jarosite; A = alunite. (Color online.)

displayed in Figure 4, with more complete results provided in Online Materials[1] Figs. S4, S5, and S8, and in Online Materials[1] Data set 1. In each panel of Figure 4, JASS in the mineralized fractures are represented by samples VoF23-19a and Vof23-25. Also included in the analyses for reference were several synthetic jarosite-alunite solid solutions (see Online Materials for synthesis methods) as well as Jurassic sandstone samples containing end-member jarosite and alunite from Mollies Nipple, Utah (Bell and Bowen 2014; Potter-McIntyre and McCollom 2018). The end-member jarosite and alunite in the Mollies Nipple (MN) samples occur as pore-filling cements in quartz-dominated sandstones with age and provenance similar to the Aztec Sandstone, and these minerals have pseudocubic morphology and size range comparable to the JASS at the study site (Online Materials[1] Fig. S9).

Analysis of representative fracture samples by XRD is shown in Online Materials[1] Figure S4, with data for additional samples provided in Online Materials[1] Data set 1. Unit-cell lattice parameters derived from the analyses are provided in Online Materials[1] Table S4 and Figure S10. The primary diagnostic XRD peaks for alunite group minerals are highlighted in Figure 4a, which shows data in the 28 to 31° range. As illustrated by the MN samples in Figure 4a, end-member alunite has a prominent peak at 29.9° (equivalent to *d*-spacing of 2.99 Å) while jarosite has a major peak at 29.0° (3.08 Å).

If the minerals in the fractures at the study site were composed of fine-scale mixtures of end-member minerals, the samples would be expected to show separate XRD peaks for both end-member minerals (e.g., Desborough et al. 2010) as seen, for example, in sample MN44 from Mollies Nipple that contains

both minerals (Fig. 4a; Online Materials[1] Fig. S9f). Instead, the VoF fracture samples display single peaks whose positions are intermediate between those of the end-member minerals, as expected for Al-Fe solid solutions (McCollom et al. 2014). For instance, sample VoF23-19a displays a peak at 29.4° (*d*-spacing = 3.035 Å), which is intermediate between those of the end-member alunite and jarosite. Moreover, the position of the peak is approximately equidistant from those of alunite and jarosite, consistent with the subequal amounts of Al and Fe for the JASS in this sample as measured by EMPA (Table 1). In addition, the peak positions for the VoF fracture samples are similar to those of synthetic solid solutions with comparable chemical compositions (Fig. 4a).

Lattice parameters for the JASS minerals calculated from the XRD results are also consistent with Al-Fe solid solutions (Online Materials[1] Fig. S10). Brophy et al. (1962) found that unit-cell dimensions for synthetic jarosite-alunite solid solutions varied linearly as a function of chemical composition, with substantially greater variability in scale for the *a* axis than for the *c* axis. As seen in Online Materials[1] Fig. S10, the unit-cell dimensions for VoF fracture samples VoF23-19a and VoF23-25 are intermediate between those of the jarosite and alunite end-members. Furthermore, the dimensions for these samples lie close to the linear trend between the end-members for the measured chemical compositions. Although the fracture samples are offset to slightly smaller cell dimensions relative to the linear jarosite-alunite trend, this is likely attributable to the presence of some hydronium in the structure since hydronium-bearing end-members have somewhat smaller dimensions (Online Materials[1] Fig. S10).

Raman spectroscopy of the alunite group minerals in the VoF fractures similarly yields features indicative of solid solutions (Fig. 4c; Online Materials[1] Fig. S5). Raman spectroscopy of synthetic natrojarosite-natroalunite solid solutions displays regular shifts in the position of many spectral bands, resulting in linear trends in band position between the pure end-members as a function of relative Al-Fe compositions (McCollom et al. 2014). Similar linear trends are expected as a function of chemical composition for jarosite-alunite solid solutions. However, so far, this has only been experimentally investigated for jarosite with a limited extent of Al-for-Fe substitution (Grigg et al. 2024). Comparison of Raman spectra for JASS in the VoF fractures with reference spectra for alunite and jarosite shows that many of the spectral bands for the VoF samples have band positions intermediate between those of pure end-members (Online Materials[1] Fig. S5). For example, alunite displays a sharp, prominent band at 1027 cm^{-1}, assigned to the υ^1 symmetric stretching mode of SO_4^{2-} units, while the equivalent band for jarosite occurs at 1006–1010 cm^{-1} (Fig. 4c; Frost et al. 2005, 2006; Grigg et al. 2024). For the JASS-bearing VoF samples and synthetic solid solutions that have comparable compositions, the positions of the equivalent bands are observed to be intermediate between the alunite and jarosite end-members, as expected for solid solutions (Fig. 4c). For the O-H stretch region between 3300 and 3600 cm^{-1}, the shape and position of the spectral features for alunite group minerals vary systematically with increasing Al-for-Fe substitution (see, for example, Fig. 5 in McCollom et al. 2014). In this region, sample VoF23-19a as well as the synthetic solid solutions display characteristics intermediate between those of the alunite and jarosite end-members, comparable to those observed in natroalunite-natrojarosite solid solutions with similar Al-Fe contents (McCollom et al. 2014).

Analyses of mineralized fracture samples by VNIR spectroscopy also produced features reflecting solid solution compositions (Fig. 4b; Online Materials[1] Fig. S8). Figure 4b shows a key diagnostic region used for detection of alunite group minerals by VNIR spectroscopy (e.g., Bell et al. 2010; Wray et al. 2011; Bell and Bowen 2014; Ehlmann et al. 2016; Leask et al. 2024). Alunite and jarosite have diagnostic VNIR absorption bands in this region at 2.17 and 2.27 μm, respectively, related to OH bending and stretching modes (Bishop and Murad 2005). Solid solutions with intermediate Al-Fe compositions exhibit both bands but also have a prominent third band at intermediate wavelengths (~2.208 μm; McCollom et al. 2014), which may be attributable to the stretching and bending modes of OH groups that bridge Al and Fe molecules. This intermediate third band is prominent in the mineralized fracture samples, as well as in the synthetic samples (Fig. 4b). The mineralized fracture samples have overall spectral shapes in the 2.1–2.4 μm range that very closely resemble those of synthetic solid solutions with similar chemical compositions but are distinctly different from those of end-member minerals (Fig. 4b).

Other alunite group minerals at the study site

Within the same general area where the mineralized fractures containing JASS were found, one fracture was observed that contained near-end-member alunite (sample VoF23-44). This mineralized fracture was white, and the pore spaces were occupied predominantly by microcrystalline (submicrometer) alunite (Online Materials[1] Figs. S11; Table 1). Jarosite and alunite were also observed sparsely distributed in a few host rocks at the same study site outside of the immediate vicinity of any JASS-mineralized fractures (Online Materials[1] Figs. S11); however, these minerals were found in only a few samples, and most of the surrounding rocks investigated contained no identifiable jarosite or alunite. In contrast to the JASS within the mineralized fractures, the jarosite and alunite found in the host rocks had near-end-member compositions (Table 1). Jarosite and alunite in the host rocks have pseudocubic habits and size ranges similar to the JASS associated with the fractures (Online Materials[1] Fig. S11). Other pore-filling minerals identified in the host rocks included small amounts of calcite, Ca-phosphates, and phyllosilicates, including kaolinite. A few Aztec Sandstone samples collected from within the boundaries of Valley of Fire State Park were also found to contain small amounts of jarosite and alunite. These minerals were too small to obtain reliable quantitative chemical analyses, and jarosite, in particular, was generally partially corroded; however, EDS analyses indicated that these occurrences had near-end-member compositions as well.

Bulk Chemistry Measurements

Bulk chemical compositions were obtained for a few samples of mineralized fractures and host rocks. Initially, these analyses were conducted on powders prepared from whole-rock hand samples. However, the resulting chemical compositions were heavily dominated by framework quartz and feldspar grains.

Therefore, to focus more on the composition of the pore-filling cement minerals, a second set of samples was analyzed using powders prepared by crushing whole-rock samples and then sieving to <53 μm to obtain fine-grained fractions for analysis. Major and minor element abundances for these samples are reported in Online Materials[1] Table S2, with additional data for trace elements provided in Online Materials[1] Data set 1. Included in the bulk chemistry data are a sample from the upper red sandstone unit within VoF State Park (Eichhubl et al. 2004), which potentially represents relatively unaltered Aztec Sandstone (sample VoF17-T25).

As expected, based on the mineralogy, the bulk chemical compositions of the mineralized fractures exhibit elevated abundances of SO_4, Al, Fe, and K (Online Materials[1] Fig. S12 and Table S2). The abundances of Fe and SO_4 far exceed the amounts originally present in the sandstones (Eichhubl et al. 2004), indicating local enrichment of these components. Because the host rocks contain several percent K-feldspar, it is not possible to determine whether the mineralized fractures are enriched in K and Al relative to the original sandstone. However, there is no clear evidence for significant dissolution of K-feldspar within the fracture zones, and the abundance of K-feldspar within the mineralized fractures appears to be similar to that of adjacent host rocks (e.g., Online Materials[1] Fig. S3b). Furthermore, there is no evidence in SEM images for accumulations of SiO_2 that would be expected if there had been extensive dissolution of K-feldspar. It appears likely, therefore, that much of the K and Al present in the JASS was transported into the mineralized fractures from elsewhere. Calcium and phosphorus also appear to be significantly enriched in most of the mineralized fractures relative to the host rocks, reflecting transport of these elements by later-stage fluids and deposition of calcite and Ca-phosphate minerals. Except for a possible increase in Sr that parallels that of Ca, there are no other minor or trace elements that clearly have higher abundances in the mineralized fractures relative to the host rock.

Isotopic composition of alunite group minerals

The isotopic compositions of S and O for sulfate in the JASS were analyzed for several mineralized fracture samples as well as one host rock that had sufficient jarosite for measurement, with results listed in Table 3. The mineralized fracture samples had $\delta^{34}S_{SO_4}$ compositions ranging from −6.6‰ to 0.1‰, which are all significantly depleted in ^{34}S relative to historic seawater values since the Jurassic (13–24‰; Claypool et al. 1980). These minerals had $\delta^{18}O_{SO_4}$ compositions ranging from 9.6‰ to 13.2‰, which is within the range of historic seawater values (7–25‰; Claypool et al. 1980). Jarosite in the host rock sample had an isotopic composition similar to the fracture samples (Table 3).

Table 3. Isotope analyses of alunite group minerals

Sample	Type	Mineral	$\delta^{34}S_{SO_4}$	$\delta^{18}O_{SO_4}$
VoF23-10	Fracture	JASS	−6.6	11.4
VoF23-19b	Fracture	JASS	0.1	10.2
VoF23-23	Fracture	JASS	−0.8	9.6
VoF23-24	Fracture	JASS	−0.3	13.2
VoF17-T11	Host rock	Jarosite	−3.3	11.7

Mössbauer and magnetic analysis of Fe-bearing minerals

To obtain additional information on JASS and other Fe-bearing minerals in the mineralized fractures, a sample from one of the fractures (VoF23-19a) was analyzed by Mössbauer spectroscopy and magnetization measurements. The MS analysis was performed on a <53 μm fraction to focus on the pore-filling minerals. The best fit to the resulting MS spectra included two doublets (Online Materials[1] Fig. S13). One doublet was assigned to the JASS and had a quadrupole shift (QS) value of 1.30 mm/s, an isomer shift (IS) of 0.37 mm/s, and accounted for 73 mol% of the Fe. The MS parameters for this doublet are consistent with those observed for synthetic Al-Fe solid solutions of alunite group minerals (McCollom et al. 2014) as well as other natural jarosite samples (Morris et al. 2006; Dyar et al. 2013). The second doublet accounted for 27 mol% of the Fe and had QS = 0.54 mm/s and IS = 0.36 mm/s. The second doublet has parameters consistent with some Fe-bearing phyllosilicates (e.g., kaolinite), several Fe-sulfates (Dyar et al. 2013), and Fe-oxide/oxyhydroxides (Murad and Johnston 1987). However, no phyllosilicates were observed in XRD or SEM analyses of the sample, and JASS was the only sulfate mineral found during extensive examination of the sample by SEM/EDS and EMPA. Conversely, Fe-oxides/oxyhydroxides were observed at sufficient abundances to account for the second doublet (Online Materials[1] Fig. S6), indicating that this doublet is most likely attributable to Fe-oxides/oxyhydroxides. This interpretation is further supported by low-temperature magnetization measurements that suggest the presence of goethite (Online Materials[1] Fig. S14). While the identity of the Fe-oxide/oxyhydroxide cannot be determined with certainty, the derived MS parameters are consistent with nanogoethite, where the doublet at 300 K represents a collapsed sextet due to superparamagnetism in nano-sized particles (Berquó et al. 2007; van der Zee et al. 2003). There was no detectable hematite in either the MS or magnetic analyses of the sample.

Discussion

Solid-solutions in the alunite-jarosite group

Analyses of the JASS found within the mineralized fractures from the Aztec Sandstone using XRD, VNIR, and Raman spectroscopy all confirm that they are bona fide solid solutions and not intimate mixtures of end-member minerals (Fig. 4). As far as the authors are aware, this is the first confirmed occurrence of solid solutions with significant Al-Fe substitution for this mineral group preserved in sedimentary rocks. This finding adds to a list of environments where solid solutions with intermediate Al-Fe compositions have been documented in natural settings that previously included only acid-sulfate fumaroles and acid-mine drainage pit lakes (Fig. 1a; McCollom et al. 2013a, 2014; Sánchez-España et al. 2016; Zhitova et al. 2022). Zuo et al. (2021) reported alunite group minerals with intermediate Al-Fe compositions in Cambrian black shales from China (their "Type II jarosite," Fig. 1a); however, the minerals they describe were analyzed using only semiquantitative energy-dispersive X-ray spectroscopy (EDS) and exhibit considerable Al-Fe zoning in elemental maps. Consequently, it is uncertain whether their analyses represent bona fide solid solutions or mixtures of

discrete, near-end-member minerals present within the analytical volume. If the report of alunite group minerals with intermediate Al-Fe compositions in Cambrian black shales by Zuo et al. (2021) can be verified by other methods to be actual solid solutions and not fine-grained mixtures of end-members (Fig. 1a), those deposits would provide additional evidence that intermediate Al-Fe solid solutions can precipitate and be preserved in sedimentary rocks.

It is not immediately apparent what conditions or circumstances allowed the alunite group minerals in the Aztec Sandstone fractures to precipitate as solid solutions rather than as separate end-member minerals. There are many localities documented in the literature where separate end-member alunite and jarosite subgroup minerals are found adjacent to one another in the same sample (e.g., Keith et al. 1979; Long et al. 1992; Alpers et al. 1992; Vasconcelos et al. 1994; Bouzari and Clark 2002; Zimbelman et al. 2005; Papike et al. 2006a, 2006b; Holley et al. 2016; Morales-Leal et al. 2023). These occurrences indicate that, even when all of the chemical ingredients to form solid solutions are present, the minerals do not always precipitate as solid solutions, and additional factors must be involved. Particularly notable in this regard are the pore-filling jarosite and alunite cements in sandstones from Mollies Nipple, which precipitated together as end-member minerals rather than as solid solutions despite a geologic setting very similar to that at VoF (Online Materials[1] Fig. S9; Potter-McIntyre and McCollom 2018).

Some studies have suggested that the co-occurrence of near-end-member alunite and jarosite may be attributable to changing environmental conditions. For example, the cooccurrence of alunite and jarosite in epithermal deposits from the Goldfield mining district in Nevada has been attributed to either: (1) a shift from Al-dominated to Fe-dominated hydrothermal fluids, or (2) a transition from reducing, circumneutral conditions that favored alunite precipitation to more oxidizing and acidic conditions that favored precipitation of jarosite (Keith et al. 1979; Papike et al. 2006a, 2006b). The latter process has been illustrated using the diagram shown in Figure 5a, where a fluid that is initially relatively reducing and mildly acidic would favor precipitation of alunite but a transition to more oxidizing and acidic conditions would favor precipitation of jarosite (it is worth noting that Figure 5a, which is redrawn from Keith et al. (1979), is actually incorrect since alunite should occupy the entire right side of the diagram and not just the lower right corner; see Online Materials[1] Fig. S15).

While explanations like those outlined above provide a rationale for why precipitation of either alunite subgroup or jarosite subgroup minerals might be preferred under certain environmental conditions, they do not really address why precipitation of solid solutions would be precluded, particularly in environments where dissolved Al, ferric Fe, and sulfate are all simultaneously available. Under such circumstances, it seems reasonable to expect that solid solutions should precipitate in natural systems, just as they do in laboratory experiments (Brophy et al. 1962; Härtig et al. 1984; Drouet et al. 2004; McCollom et al. 2014). Precipitation of solid solutions would also appear to be favored based on thermodynamics, as illustrated in Figure 5b. This figure shows a mineral stability diagram in which an example solid solution with a composition intermediate between jarosite and alunite has been included among the minerals considered in the construction of the diagram, assuming an ideal mixing model for the solid solution (see Online Materials[1]). It can be seen in the figure that the solid solution occupies a large portion of the diagram, which lies between end-member jarosite and alunite, indicating that precipitation of solid solutions should be favored over that of

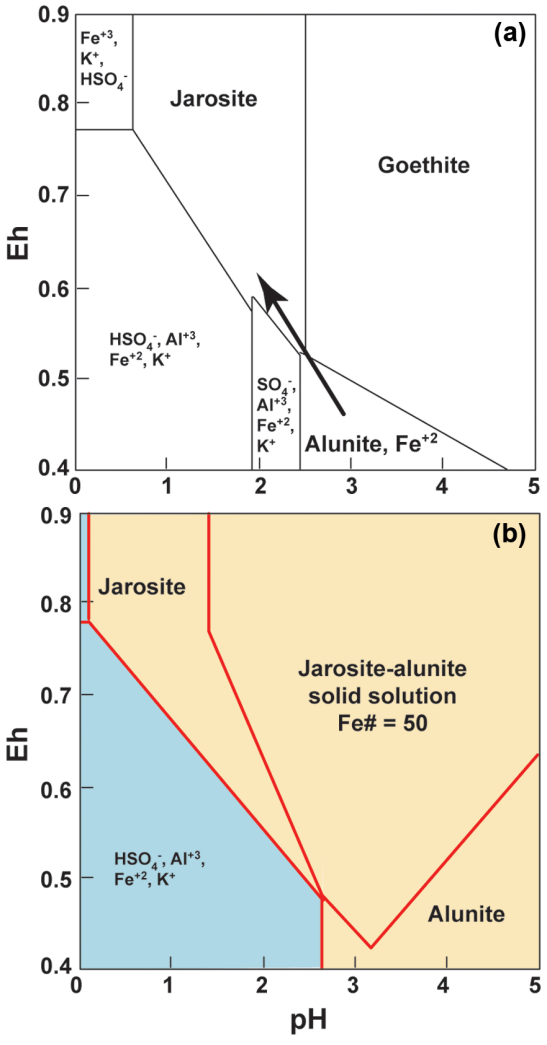

Figure 5. Mineral stability diagrams for the system Al-Fe-K-SO_4-H_2O. (**a**) Stability diagram redrawn after Keith et al. (1979) and Papike et al. (2006b). Arrow illustrates their nominal pathway for transition from conditions favoring alunite precipitation to those favoring jarosite precipitation. (**b**) Analogous diagram that includes a representative jarosite-alunite solid solution that has a composition intermediate between jarosite and alunite end-members. The diagram in (**b**) was constructed with Geochemist's Workbench using the thermo.com.V8.R6+ database modified to include the solid solution, using estimated thermodynamic parameters as described in the Online Materials[1]. Following Keith et al. (1979), both diagrams assume $a_{\Sigma Fe} = 10^{-1}$, $a_{Al} = 10^{-3}$, $a_{SO_4} = 10^{-2}$, and $a_K = 10^{-3}$. The calculations are for 25 °C and 1 bar. Both diagrams exclude hematite, and (**b**) also excludes goethite, which precludes the formation of the solid solution. Diaspore is stable relative to alunite for pH > ~4.9 at the specified conditions but has been excluded from the diagrams for simplicity. (Color online.)

the end-members for conditions in the upper right part of the diagram. Therefore, any transition in environmental conditions from relatively reducing to oxidizing, or a lowering of pH, would traverse the stability field of the solid solution and should lead to precipitation of a solid solution rather than end-member components. Yet, there are many environments where alunite subgroup and jarosite subgroup minerals co-precipitate with near-end-member compositions rather than forming solid solutions, including epithermal deposits (Keith et al. 1979; Papike et al. 2006a, 2006b; Morales-Leal et al. 2023), acid-saline lake sediments (Long et al. 1992; Alpers et al. 1992), volcanic deposits (Zimbelman et al. 2005), and the Jurassic sandstone cements at Mollies Nipple (Online Materials[1] Fig. S9) (Bell and Bowen 2014; Potter-McIntyre and McCollom 2018).

Sánchez-España et al. (2016) report the occurrence of JASS with a range of chemical compositions intermediate between jarosite and alunite in acid-mine pit lakes in Spain (Fig. 1a). They propose that the solid solutions precipitate as a result of variable environmental conditions within the lakes. At pH > ~4.4, dissolved Al derived from the acid-mine drainage precipitates as Al-sulfate or Al-hydroxide minerals; however, at lower pH these minerals are thermodynamically unstable so that Al remains dissolved and is thus available to precipitate along with ferric Fe minerals, including JASS with intermediate compositions. In this case, the circumstances that led to precipitation of Al-Fe solid solutions include: (1) conditions that are sufficiently oxidizing to allow dissolved Fe to be present as Fe^{3+} rather than Fe^{2+}; (2) a substantial source of both dissolved Fe and Al as well as sulfate; and (3) a pH below ~4. It is certainly feasible that such conditions were met during the deposition of JASS in the mineralized fractures in the Aztec Sandstone. However, it is not yet clear whether additional factors may have been involved that led to the precipitation of solid solutions rather than separate near-end-member minerals in these environments.

Prior to the present study, one possible alternative explanation for the scarcity of Al-Fe solid solutions in natural samples (Fig. 1a) was that they may be able to precipitate but are inherently unstable over longer timescales. That is, intermediate Al-Fe solid solutions might initially precipitate but then decompose over time, perhaps through exsolution into separate end-member components (Desborough et al. 2010), thereby precluding the preservation of these solid solutions in the geological record. In this regard, it is worth noting that previously identified cases of Al-Fe solid solutions had been limited to environments where the minerals have a relatively recent origin (i.e., active fumaroles and acid-mine pit lakes), and they might not persist in these environments long enough to be preserved in the geologic record.

However, the occurrence of Al-Fe solid solutions in the Aztec Sandstone demonstrates that they can persist for extended periods. The age of deposition of the JASS in the fractures is presently uncertain, but they likely formed at least several million years ago. Faults in the Aztec Sandstone are thought to have initially formed during Late Cretaceous Sevier thrusting (Taylor et al. 1999; Flodin et al. 2004; Eichhubl et al. 2004), which places an upper limit on the age of mineralization. However, the mineralization of the fractures at the study site may have occurred at a more recent time, and Eichhubl et al. (2004) inferred that the jarosite and alunite in the Aztec Sandstone within Valley of Fire State Park were deposited during fluid flow associated with Basin and Range tectonics in the Miocene. The JASS mineralization at the study site south of the park may well have been deposited during this same period, and if so, the solid solutions have persisted for at least several million years. Potassium-argon dating of the JASS in future studies could potentially provide more robust constraints on their age (Keith et al. 1979; Stoffregen et al. 2000).

Precipitation of jarosite-alunite solid-solutions in the mineralized fractures

Further investigation will be necessary to fully understand the chemical environment and circumstances that lead to the precipitation of Al-Fe solid solutions in the mineralized fractures. However, some preliminary constraints can be inferred from the currently available data. It is generally thought that precipitation of jarosite subgroup minerals requires a pH of less than about 4.5, while alunite subgroup minerals can potentially precipitate to somewhat higher pH (e.g., Keith et al. 1979; Papike et al. 2006a, 2006b; Sánchez-España et al. 2016). The upper limits of pH values that allow the precipitation of Al-Fe solid solutions are currently uncertain, as laboratory syntheses of solid solutions have only been conducted under strongly acidic conditions (Brophy et al. 1962; Härtig et al. 1984; Drouet et al. 2004; McCollom et al. 2014). The preliminary calculations shown in Figure 5c suggest that solid solutions may be thermodynamically favored over end-member compositions across a broad pH range when both Al and Fe are available in the environment. However, it should be emphasized that the mineral stability boundaries in this particular diagram are dependent on the activities of dissolved species assumed in the calculations. In any event, it appears likely that the fluids which precipitated the JASS in the mineralized fractures were at least mildly acidic. Precipitation of Fe-rich JASS also requires relatively oxidizing conditions, since more reducing conditions would favor precipitation of ferrous sulfate minerals (e.g., Papike et al. 2006a, 2006b; Sánchez-España et al. 2016) or sulfide minerals rather than sulfates.

The amount of Fe and S available locally in the fractures themselves is insufficient to account for the JASS mineralization (e.g., Eichhubl et al., 2004), indicating that Fe and S must be transported into the mineralized fractures by migrating fluids. The original Aztec Sandstone likely contained small amounts of Fe as coatings on sand grains (Eichhubl et al. 2004), and the surrounding rocks may have supplied some of the Fe to form the JASS in the fractures. However, basinal fluids were likely required as a source of S, and these fluids may have also contributed some of the Fe. The original sandstones contained abundant K-feldspar (Eichhubl et al. 2004), and the K_2O:Al_2O_3 ratios in the mineralized fractures parallel those of this mineral (Online Materials[1] Fig. S12d). This suggests that the K and Al required for the formation of the JASS are probably derived from feldspar dissolution, either within the mineralized fractures themselves or from the surrounding host rocks.

Eichhubl et al. (2004) proposed that the small amounts of end-member jarosite and alunite found in some Aztec Sandstone rocks within the boundaries of VoF formed when reduced and acidic basinal fluids containing dissolved Fe and S mixed with more oxidized shallow meteoritic water. The oxidation of

dissolved Fe and S, as the fluids mixed, would have led to conditions that favored the precipitation of jarosite and alunite, with K and Al presumably derived from the dissolution of K-feldspar. Note that precipitation of alunite group minerals from solution generates acidity according to the general reaction:

$$K^+ + 3xFe^{3+} + 3yAl^{3+} + 2SO_4^{2-} + 6\,H_2O \rightarrow K(Fe_xAl_y)_3(SO_4)_2(OH)_6 + 6H^+ \quad (1)$$

where $y = 1 - x$. While some H^+ may be consumed by dissolution of K-feldspar to create dissolved K^+ and Al^{3+}, as well as during oxidation of Fe^{2+}, the net result would still be a local increase in acidity when minerals from this group precipitate from solution.

A similar mixing scenario could account for the precipitation of JASS deposits in the mineralized fractures investigated for this study, as well as the precipitation of the more sparsely distributed end-member jarosite and alunite in the surrounding host rocks at the study site. The higher permeability associated with the fractures makes them a locus of increased fluid flux (e.g., Taylor et al. 1999), which may have led to more intense mixing and greater mineral precipitation, accounting for the high density of pore-filling JASS in the mineralized fractures. The intensity of oxidation reactions within the fractures may have also provided a localized environment with simultaneously abundant Fe^{3+}, Al, and SO_4, which favored the precipitation of minerals as solid solutions rather than as separate end-members. Increased acidity produced through reaction 1 in this localized environment may also have contributed to precipitation of the minerals as solid solutions rather than two separate end-members.

A basinal source of the S in the fluids would be consistent with the isotopic composition of the JASS (Table 3). The S in the JASS is substantially depleted in ^{34}S relative to seawater, dating back to the Jurassic (Claypool 1980), as well as to gypsum deposits in other sedimentary rocks in the region (Chen et al. 2016), indicating that the sulfate must be derived from a source not directly connected to seawater. Although the S and O isotopic compositions of the JASS are similar to alunite group minerals formed by steam-heating of sulfides in supergene ore deposits (e.g., Rye 2005), there is no evidence for volcanic or hydrothermal activity in the vicinity of the study site, and the precursor rocks contained essentially no sulfide minerals. Thus, there is no reason to believe that analogous processes could have provided a source of sulfate for the JASS. Whatever the ultimate source is, reduced S in basinal fluids is likely to have an isotopic composition that is more depleted in ^{34}S than seawater (or from dissolution of sulfate minerals derived from ancient seawater). The similarity of the isotopic composition of jarosite in the host rock to that of the mineralized fractures (Table 3) suggests that the S for both types of mineral deposits came from the same source.

The nature of the putative basinal fluids was not described in detail by Eichhubl et al. (2004), but one possibility is that they were organic-rich and that this promoted the formation of the JASS. Organic acid anions, such as acetate and propionate in the fluids, could have facilitated the reduction and transport of ferrous Fe from underlying units, while dissolved H_2S and organosulfur compounds could have provided a source of sulfate when the fluids were oxidized. This possibility is potentially supported by the widespread presence of bituminous carbonaceous matter in the pore spaces of diagenetically altered Aztec Sandstone samples collected within VoF State Park (Online Materials[1] Fig. S16). This bitumen is highly enriched in sulfur (e.g., Online Materials Fig. S16e) that, once oxidized, could have potentially served as a source of sulfate for the JASS. An organic source would also be consistent with the ^{34}S-depleted isotopic composition of sulfate in the minerals (Orr 1974; Amrani 2014). Although no bituminous deposits were found in the samples from the area south of VoF examined for this study, the organic matter could have been transported out of the rocks at a later time or simply failed to accumulate locally in the rocks at the study site.

Another possible scenario for the origin of the JASS in the mineralized fractures is that they are products of remobilization of jarosite and alunite from the surrounding host rocks. The initial precipitation of jarosite and alunite in the host rocks may have resulted from mixing of oxidizing and reducing fluids, as proposed by Eichhubl et al. (2004) elsewhere in the Aztec Sandstone. Changing conditions over time, however, may have caused these minerals to become unstable and redissolve, and the dissolved components could have then been transported to the fracture zones where they reprecipitated as solid solutions. Evidence that might support this interpretation includes the similar isotope compositions of alunite group minerals in the host rocks and mineralized fractures (Table 3), and apparent dissolution textures of jarosite within some of the host rocks in the immediate vicinity of the mineralized fractures (Online Materials[1] Fig. S11).

At this juncture, the full range of circumstances that led to formation of Al-Fe solid solutions in the Aztec Sandstones remains obscure. While the environment that allowed the formation of solid solutions in the mineralized fractures certainly shares some common characteristics with the other environments where solid solutions of alunite group minerals have been found (e.g., high acidity, oxidizing conditions, presence of sulfate), the settings for these occurrences are quite different. A detailed comparison of the Aztec Sandstone samples with those from other localities where Al-Fe solid solutions have been documented (acid-sulfate fumaroles, acid-mine pit lakes) may provide additional insight into why the alunite group minerals in these environments precipitated as solid solutions rather than end-member minerals.

Implications

Until very recently, it was generally thought that solid solutions of alunite group minerals with intermediate Al-Fe compositions did not exist in natural settings (e.g., Scott 1987; Stoffregen et al. 2000; Papike et al. 2006a, 2006b). The results reported here, combined with other recent reports on volcanic fumaroles and mine-drainage pit lakes, provide increasing evidence that intermediate solid solutions do exist in nature. These findings may necessitate a reconsideration of the crystal chemistry of this widespread mineral group and could provide new insights into the environmental conditions present when alunite

group minerals precipitate as solid solutions, as well as when they co-precipitate with near-end-member compositions. The findings may also stimulate the discovery of intermediate Al-Fe in other geologic settings.

One locality where these results may have immediate relevance is the planet Mars. Using Mössbauer spectroscopy, the Mars Exploration Rover Opportunity discovered the presence of jarosite subgroup minerals in the layered, sulfate-rich sandstones of the Burns Formation on Meridiani Planum (Klingelhöfer et al. 2004; Morris et al. 2006). Although commonly referred to as jarosite, elemental mass balance and other considerations indicate that the minerals present on Meridiani are actually Al-rich natrojarosites (Morris et al. 2006). Further studies of intermediate Al-Fe solid solutions among alunite group minerals in the Aztec Sandstone and elsewhere may therefore lead to new insights into environmental conditions during formation and diagenesis of the Burns sandstones. Moreover, the ability of methods such as XRD, VNIR spectroscopy, and Raman spectroscopy to detect Al-Fe solid solutions without the need to make micrometer-scale chemical measurements may lead to additional detections of such solid solutions on Mars and elsewhere.

Acknowledgments and Funding

This research was supported by the NASA Solar System Workings program through award number 80NSSC19K0552. The IRM is a U.S. National Multi-user Facility supported through the Instrumentation and Facilities program of the National Science Foundation, Earth Sciences Division (EAR-2153786), and by funding from the University of Minnesota. This is IRM contribution #2404. We thank Jessica Hankins for assistance with Raman measurements and Janice Bishop for discussion of VNIR spectroscopy of alunite group minerals. The authors are grateful for three anonymous reviewers whose comments helped improve the manuscript. Samples within the Valley of Fire State Park were collected under a research permit issued to S.P.-M. and T.M.M.

References Cited

Alpers, C.N., Rye, R.O., Nordstrom, D.K., White, D.L., and King, B.-S. (1992) Chemical, crystallographic and stable isotopic properties of alunite and jarosite from acid-hypersaline Australian lakes. Chemical Geology, 96, 203–226, https://doi.org/10.1016/0009-2541(92)90129-S.

Amrani, A. (2014) Organosulfur compounds: Molecular and isotopic evolution from biota to oil and gas. Annual Review of Earth and Planetary Sciences, 42, 733–768, https://doi.org/10.1146/annurev-earth-050212-124126.

Basciano, L.C. and Peterson, R.C. (2007) Jarosite-hydronium jarosite solid-solution series with full iron site occupancy: Mineralogy and crystal chemistry. American Mineralogist, 92, 1464–1473, https://doi.org/10.2138/am.2007.2432.

——— (2008) Crystal chemistry of the natrojarosite-jarosite and natrojarosite-hydronium jarosite solid-solution series: A synthetic study with full Fe site occupancy. American Mineralogist, 93, 853–862, https://doi.org/10.2138/am.2008.2731.

Bell, J.H. and Bowen, B.B. (2014) Fracture-focused fluid flow in an acid and redox-influenced system: Diagenetic controls on cement mineralogy and geomorphology in the Navajo Sandstone. Geofluids, 14, 251–265, https://doi.org/10.1111/gfl.12075.

Bell, J.H., Bowen, B.B., and Martini, B.A. (2010) Imaging spectroscopy of jarosite cement in the Jurassic Navajo Sandstone. Remote Sensing of Environment, 114, 2259–2270, https://doi.org/10.1016/j.rse.2010.05.002.

Berqué, T.S., Imbernon, R.A.L., Blot, A., Franco, D.R., Toledo, M.C.M., and Partiti, C.S.M. (2007) Low temperature magnetism and Mössbauer spectroscopy study from natural goethite. Physics and Chemistry of Minerals, 34, 287–294, https://doi.org/10.1007/s00269-007-0147-9.

Bishop, J.L. and Murad, E. (2005) The visible and infrared spectral properties of jarosite and alunite. American Mineralogist, 90, 1100–1107, https://doi.org/10.2138/am.2005.1700.

Bouzari, F. and Clark, A.H. (2002) Anatomy, evolution, and metallogenic significance of the supergene orebody of the Cerro Colorado porphyry copper deposit, I Región, Northern Chile. Economic Geology, 97, 1701–1740.

Brophy, G.P. and Sheridan, M.F. (1965) Sulfate studies IV: The jarosite-natrojarosite-hydronium jarosite solid solution series. American Mineralogist, 50, 1595–1607.

Brophy, G.P., Scott, E.S., and Snellgrove, R.A. (1962) Sulfate studies II: Solid solution between alunite and jarosite. American Mineralogist, 47, 112–126.

Burger, P.V., Papike, J.J., Shearer, C.K., and Karner, J.M. (2009) Jarosite growth zoning as a recorder of fluid evolution. Geochimica et Cosmochimica Acta, 73, 3248–3259, https://doi.org/10.1016/j.gca.2009.02.031.

Cao, F., Ling, Z., and Ni, Y. (2017) Chemical and spectroscopic investigations of K-H_3O-Na jarosite solid solutions applicable for Mars explorations. Journal of Raman Spectroscopy, 48, 1544–1553, https://doi.org/10.1002/jrs.5222.

Chen, F., Turchyn, A.V., Kampman, N., Hodell, D., Gázquez, F., Maskell, A., and Bickle, M. (2016) Isotopic analysis of sulfur cycling and gypsum vein formation in a natural CO_2 reservoir. Chemical Geology, 436, 72–83, https://doi.org/10.1016/j.chemgeo.2016.04.015.

Claypool, G.E., Holser, W.T., Kaplan, I.R., Sakai, H., and Zak, I. (1980) The age curves of sulfur and oxygen isotopes in marine sulfate and their mutual interpretation. Chemical Geology, 28, 199–260, https://doi.org/10.1016/0009-2541(80)90047-9.

Desborough, G.A., Smith, K.S., Lowers, H.A., Swayze, G.A., Hammarstrom, J.M., Diehl, S.F., Leinz, R.W., and Driscoll, R.L. (2010) Mineralogical and chemical characteristics of some natural jarosites. Geochimica et Cosmochimica Acta, 74, 1041–1056, https://doi.org/10.1016/j.gca.2009.11.006.

Deyell, C.L. and Dipple, G.M. (2005) Equilibrium mineral-fluid calculations and their application to solid solution between alunite and natroalunite in the El Indio-Pascua belt of Chile and Argentina. Chemical Geology, 215, 219–234, https://doi.org/10.1016/j.chemgeo.2004.06.039.

Drouet, C., Pass, K.L., Baron, D., Draucker, S., and Navrotsky, A. (2004) Thermochemistry of jarosite-alunite and natrojarosite-natroalunite solid solutions. Geochimica et Cosmochimica Acta, 68, 2197–2205, https://doi.org/10.1016/j.gca.2003.12.001.

Dutrizac, J.E. and Jambor, J.L. (2000) Jarosites and their application in hydrometallurgy. Reviews in Mineralogy and Geochemistry, 40, 405–452, https://doi.org/10.2138/rmg.2000.40.8.

Dyar, M.D., Breves, E., Jawin, E., Marchand, G., Nelms, M., O'Connor, V., Peel, S., Rothstein, Y., Sklute, E.C., Lane, M.D., and others. (2013) Mössbauer parameters of iron in sulfate minerals. American Mineralogist, 98, 1943–1965, https://doi.org/10.2138/am.2013.4604.

Ehlmann, B.L., Swayze, G.A., Milliken, R.E., Mustard, J.F., Clark, R.N., Murchie, S.L., Breit, G.N., Wray, J.J., Gondet, B., Poulet, F., and others. (2016) Discovery of alunite in Cross Crater, Terra Sirenum, Mars: Evidence for acidic, sulfurous waters. American Mineralogist, 101, 1527–1542, https://doi.org/10.2138/am-2016-5574.

Eichhubl, P., Taylor, W.L., Pollard, D.D., and Aydin, A. (2004) Paleo-fluid flow and deformation in the Aztec Sandstone at the Valley of Fire, Nevada—Evidence for the coupling of hydrologic, diagenetic, and tectonic processes. Geological Society of America Bulletin, 116, 1120–1136, https://doi.org/10.1130/B25446.1.

Flodin, E.A. and Aydin, A. (2004a) Evolution of a strike-slip fault network. Valley of Fire State Park. GSA Bulletin, 116, 42–59.

——— (2004b) Faults with asymmetric damage zones in sandstone, Valley of Fire State Park, southern Nevada. Journal of Structural Geology, 26, 983–988, https://doi.org/10.1016/j.jsg.2003.07.009.

Frost, R.L., Wills, R.-A., Weier, M.L., and Martens, W. (2005) Comparison of the Raman spectra of natural and synthetic K- and Na-jarosites at 298 and 77 K. Journal of Raman Spectroscopy, 36, 435–444, https://doi.org/10.1002/jrs.1317.

Frost, R.L., Wills, R.-A., Weier, M.L., Martens, W., and Kloprogge, J.T. (2006) A Raman spectroscopic study of alunites. Journal of Molecular Structure, 785, 123–132, https://doi.org/10.1016/j.molstruc.2005.10.003.

Grigg, A.R.C., Notini, L., Kaegi, R., ThomasArrigo, L.K., and Kretzschmar, R. (2024) Structural effects of aluminum and iron occupancy in minerals of the jarosite-alunite solid solution. ACS Earth & Space Chemistry, 8, 194–206, https://doi.org/10.1021/acsearthspacechem.3c00174.

Härtig, C., Brand, P., and Bohmhammel, K. (1984) Fe-Al-Isomorphie und Strukturwasser in Kristallen vom Jarostie-Alunit-Typ. Zeitschrift für Anorganische und Allgemeine Chemie, 508, 159–164, https://doi.org/10.1002/zaac.19845080123.

Holley, E.A., Bissig, T., and Monecke, T. (2016) The Valdero high-sulfidation epithermal gold deposit, El Indio-Pascua Belt, Argentina: Geochronology of alunite and jarosite. Economic Geology and the Bulletin of the Society of Economic Geologists, 111, 311–330, https://doi.org/10.2113/econgeo.111.2.311.

Jambor, J.L. (1999) Nomenclature of the alunite supergroup. Canadian Mineralogist, 37, 1323–1341.

Juliani, C., Rye, R.O., Nunes, C.M.D., Snee, L.W., Corrêa Silva, R.H., Monteiro, L.V.S., Bettencourt, J.S., Neumann, R., and Alcover Neto, A. (2005) Paleoproterozoic high-sulfidation mineralization in the Tapajós gold province, Amazonian Craton, Brazil: Geology, mineralogy, alunite argon age, and stable-isotope constraints. Chemical Geology, 215, 95–125, https://doi.org/10.1016/j.chemgeo.2004.06.035.

Keith, K.J., Calk, L., and Ashley, R.P. (1979) Crystals of coexisting alunite and jarosite, Goldfield, Nevada. USGS Professional Paper 1124-C.

Klingelhöfer, G., Morris, R.V., Bernhardt, B., Schröder, C., Rodionov, D.S., de Souza, P.A. Jr., Yen, A., Gellert, R., Evlanov, E.N., Zubkov, B., and others.

(2004) Jarosite and hematite at Meridiani Planum from Opportunity's Mossbauer Spectrometer. Science, 306, 1740–1745, https://doi.org/10.1126/science.1104653.
Leask, E. K., Ehlmann, B. L., and Dundar, M. M. (2024) A 2-billion-year history of water-alteration in Terra Sirenum, Mars: Volcanism's influence on aluminum clay formation and chemically distinct waters forming sulfates and chlorides in the Amazonian. JGR: Planets, 129, e2023JE008259.
Long, D.T., Fegan, N.E., McKee, J.D., Lyons, W.B., Hines, M.E., and Macumber, P.G. (1992) Formation of alunite, jarosite and hydrous iron oxides in a hypersaline system: Lake Tyrell, Victoria, Australia. Chemical Geology, 96, 183–202, https://doi.org/10.1016/0009-2541(92)90128-R.
McCollom, T.M. (2024) Chemical compositions of minerals from the alunite-jarosite group compiled from the literature. Zenodo, https://doi.org/10.5281/zenodo.10660117.
McCollom, T.M., Hynek, B.M., Rogers, K., Moskowitz, B., and Berquó, T.S. (2013a) Chemical and mineralogical trends during acid-sulfate alteration of pyroclastic basalt at Cerro Negro volcano and implications for early Mars. JRG: Planets, 118, 1719–1751, https://doi.org/10.1002/jgre.20114.
McCollom, T.M., Robbins, M., Moskowitz, B., Berquó, T.S., Jöns, N., and Hynek, B.M. (2013b) Experimental study of acid-sulfate alteration of basalt and implications for sulfate deposits on Mars. JGR: Solid Earth, 118, 1–38.
McCollom, T.M., Ehlmann, B.L., Wang, A., Hynek, B.M., and Berquó, T.S. (2014) Detection of iron substitution in natroalunite-natrojarosite solid solutions and potential implications for Mars. American Mineralogist, 99, 948–964, https://doi.org/10.2138/am.2014.4617.
Mills, S.J., Hatert, F., Nickel, E.H., and Ferraris, G. (2009) The standardization of mineral group hierarchies. European Journal of Mineralogy, 21, 1073–1080, https://doi.org/10.1127/0935-1221/2009/0021-1994.
Morales-Leal, J.E., Campos, E., Kouzmanov, K., and Riquelme, R. (2023) Alunite supergroup minerals from advanced argillic alteration assemblage in the southern Atacama Desert as indicators of paleo-hydrothermal and supergene environments. Mineralium Deposita, 58, 593–615, https://doi.org/10.1007/s00126-022-01149-5.
Morris, R.V., Klingelhöfer, G., Schröder, C., Rodionov, D.S., Yen, A., Ming, D.W., de Souza, P.A. Jr., Wdowiak, T., Fleischer, I., Gellert, R., and others. (2006) Mössbauer mineralogy of rock, soil, and dust at Meridiani Planum, Mars: Opportunity's journey across sulfate-rich outcrop, basaltic sand and dust, and hematite lag deposits. Journal of Geophysical Research: Planets, 111, E12S15, https://doi.org/10.1029/2006JE002791.
Murad, E. and Johnston, J.H. (1987) Iron oxides and oxyhydroxides. In G.J. Long, Ed., Mössbauer Spectroscopy Applied to Inorganic Chemistry, p. 507–582. Plenum.
Orr, W.L. (1974) Changes in sulfur content and isotopic ratios of sulfur during petroleum maturation—Study of Big Horn Basin Paleozoic oils. The American Association of Petroleum Geologists Bulletin, 58, 2295–2318.
Papike, J.J., Karner, J.M., Spilde, M.N., and Shearer, C.K. (2006a) Terrestrial analogs of martian sulfates: Major and minor element systematics of alunitde-jarosite from Goldfield, Nevada. American Mineralogist, 91, 1197–1200, https://doi.org/10.2138/am.2006.2257.
Papike, J.J., Karner, J.M., and Shearer, C.K. (2006b) Comparative planetary mineralogy: Implications of martian and terrestrial jarosite. A crystal chemical perspective. Geochimica et Cosmochimica Acta, 70, 1309–1321, https://doi.org/10.1016/j.gca.2005.11.004.
Papike, J.J., Burger, P.V., Karner, J.M., Shearer, C.K., and Lueth, V.W. (2007) Terrestrial analogs of martian jarosites: Major, minor element systematics and Na-K zoning in selected samples. American Mineralogist, 92, 444–447, https://doi.org/10.2138/am.2007.2442.
Polyak, V.J. and Güven, N. (1996) Alunie, natroalunite and hydrated halloysite in Carlsbad Cavern and Lechuguilla Cave, New Mexico. Clays and Clay Minerals, 44, 843–850, https://doi.org/10.1346/CCMN.1996.0440616.
Potter-McIntyre, S.L. and McCollom, T.M. (2018) Jarosite and alunite in ancient terrestrial sedimentary rocks: Reinterpreting martian depositional and diagenetic environmental conditions. Life, 8, 32, https://doi.org/10.3390/life8030032.
Ripmeester, J.A., Ratcliffe, C.I., Dutrizac, J.E., and Jambor, J.L. (1986) Hydronium ion in the alunite-jarosite group. Canadian Mineralogist, 24, 435–447.
Rye, R.O. (2005) A review of the stable-isotope geochemistry of sulfate minerals in selected igneous environments and related hydrothermal systems. Chemical Geology, 215, 5–36, https://doi.org/10.1016/j.chemgeo.2004.06.034.
Sánchez-España, J., Yusta, I., Gray, W., and Burgos, W.D. (2016) Geochemistry of dissolved aluminum at low pH: Extent and significance of Al-Fe(III) coprecipitation below pH 4.0. Geochimica et Cosmochimica Acta, 175, 128–149, https://doi.org/10.1016/j.gca.2015.10.035.
Scott, K.M. (1987) Solid solution in, and classification of, gossan-derived members of the alunite-jarosite family, northwest Queensland, Australia. American Mineralogist, 72, 178–187.
Stoffregen, R.E. and Alpers, C.N. (1992) Observations on the unit-cell dimensions, H_2O contents, and δD values of natural and synthetic alunite. American Mineralogist, 77, 1092–1098.
Stoffregen, R.E. and Cygan, G.L. (1990) An experimental study of Na-K exchange between alunite and aqueous sulfate solutions. American Mineralogist, 75, 209–220.
Stoffregen, R.E., Alpers, C.N., and Jambor, J.L. (2000) Alunite-jarosite crystallography, thermodynamics, and geochronology. Reviews in Mineralogy and Geochemistry, 40, 453–479, https://doi.org/10.2138/rmg.2000.40.9.
Talla, D. and Wildner, M. (2019) Investigation of the kieserite-szomolnokite solid-solution series, $(Mg,Fe)SO_4 \cdot H_2O$, with relevance to Mars: Crystal chemistry, FTIR, and Raman spectroscopy under ambient and martian temperature conditions. American Mineralogist, 104, 1732–1749, https://doi.org/10.2138/am-2019-6983.
Talla, D., Balla, M., Aicher, C., Lengauer, C.L., and Wildner, M. (2020) Structural and spectroscopic study of the kieserite-dwornikite solid-solution series, $(Mg,Ni)SO_4 \cdot H_2O$, at ambient and low temperatures, with cosmochemical implications for icy moons and Mars. American Mineralogist, 105, 1472–1489, https://doi.org/10.2138/am-2020-7287.
Taylor, W.L. and Pollard, D.D. (2000) Estimation of in situ permeability of deformation bands in porous sandstone, Valley of Fire, Nevada. Water Resources Research, 36, 2595–2606, https://doi.org/10.1029/2000WR900120.
Taylor, W.L., Pollard, D.D., and Aydin, A. (1999) Fluid flow in discrete joint sets: Field observations and numerical simulations. JGR: Solid Earth, 104, 28 983–29 006, https://doi.org/10.1029/1999JB900179.
van der Zee, C., Roberts, D.R., Rancourt, D.G., and Slomp, C.P. (2003) Nanogoethite is the dominant reactive oxyhydroxide phase in lake and marine sediments. Geology, 31, 993–996, https://doi.org/10.1130/G19924.1.
Vasconcelos, P.M., Brimhall, G.H., Becker, T.A., and Renne, P.R. (1994) $^{40}Ar/^{39}Ar$ analysis of supergene jarosite and alunite: Implications for the paleoweathering history of the western USA and West Africa. Geochimica et Cosmochimica Acta, 58, 401–420, https://doi.org/10.1016/0016-7037(94)90473-1.
Vegard, L. (1921) Die constitution der mischkristalle und die raumfüllung der atome. The European Physical Journal A, 5, 17–26, https://doi.org/10.1007/BF01349680.
Whitworth, A.J., Brand, H.E.A., Wilson, S.A., and Frierdich, A.J. (2020) Iron isotope geochemistry and mineralogy of jarosite in sulfur-rich sediments. Geochimica et Cosmochimica Acta, 270, 282–295, https://doi.org/10.1016/j.gca.2019.11.029.
Wray, J.J., Milliken, R.E., Dundas, C.M., Swayze, G.A., Andrews-Hanna, J.C., Baldridge, A.M., Chojnacki, M., Bishop, J.L., Ehlmann, B.L., Murchie, S.L., and others. (2011) Columbus crater and other possible groundwater-fed paleolakes of Terra Sirenum, Mars. JGR: Solid Earth, 116, E01001, https://doi.org/10.1029/2010JE003694.
Zhitova, E.S., Khanin, D.A., Nuzhdaev, A.A., Nazarova, M.A., Ismagilova, R.M., Shilovskikh, V.V., Kupchinenko, A.N., Kuznetsov, R.A., and Zhegunov, P.S. (2022) Efflorescent sulphates with M^+ and M^{2+} cations from fumarole and active geothermal fields from Mutnovsky Volcano (Kamchatka, Russia). Minerals, 12, 600, https://doi.org/10.3390/min12050600.
Zimbelman, D.R., Rye, R.O., and Breit, G.N. (2005) Origin of secondary sulfate minerals on active andesitic stratovolcanoes. Chemical Geology, 215, 37–60, https://doi.org/10.1016/j.chemgeo.2004.06.056.
Zuo, P., Sun, J., Liu, X., Hao, J., and Li, Y. (2021) Two types of jarosite in the early Cambrian sedimentary rocks: Insights for genesis and transformation of jarosite on Mars. Icarus, 369, 114651, https://doi.org/10.1016/j.icarus.2021.114651.

Manuscript received April 12, 2024
Manuscript accepted February 14, 2025
Accepted manuscript online February 27, 2025
Manuscript Handled by Lindsay J. McHenry

Endnotes:

[1]Deposit item AM-25-109423. Online Materials are free to all readers. Go online, via the table of contents or article view, and find the tab or link for supplemental materials.